

# Effects of Grain Size on the UV-Photoresponse of Zinc Oxide Thin Films Grown by Spray-Pyrolysis

Edgar A. Villegas, Celso M. Aldao, Raluca Savu, Leandro A. Ramajo, and Rodrigo Parra\*

Zinc oxide films with different average grain size are deposited on glass substrates by spray-pyrolysis at 425 °C. Samples are characterized by XRD, UV-Vis transmittance, FE-SEM, and electrical properties measurements. The increase in conductivity observed under 365 nm wavelength illumination is evaluated in terms of grain size. Films with small grains (120 nm) show higher response with respect to films with larger grains (230 and 300 nm). A model considering resistivity and grain size for the prediction of the response of films in terms of UV-to-dark conductivity ratio is proposed and validated with experimental results.

## 1. Introduction

Zinc oxide-based materials are among the most widely investigated ceramics. The physico-chemical properties of this oxide determine its suitability for diverse applications which range from cosmetic and biomedical products to (micro) electronic and optical devices. Zinc oxide (ZnO) is an n-type semiconductor with a wide direct band-gap of about 3.37 eV, conferring the ultraviolet radiation (UV) filtering properties required for its widespread use in sunscreen lotions.<sup>[1]</sup> Moreover, because of its transparency in the visible region of the electromagnetic spectrum, ZnO is appropriate for low emissivity coatings and efficient windows. Intrinsic ZnO as a thin film exhibits oxygen deficiency that introduces defect states in the electronic structure of the material. Because defects may affect the performance of the device, addition of oxygen into deposition chambers is sometimes practiced in order to control stoichiometry and defect formation.<sup>[2]</sup> However, by decreasing the electrical resistivity by means of extrinsic defects generated by donor doping, ZnO films turn into transparent conductive oxides (TCO) with

applications of increasing technological interest such as transparent electrodes, solar cell anodes, light emitting diodes, liquid crystal displays, and touch-screens, among others.<sup>[3–5]</sup> Another interesting application that has gained attention is the use of ZnO in UV photodetectors for safety devices, flame detection, optical communication, industrial packaging/sealing lines and monitoring of artificially illuminated working environments.<sup>[6–10]</sup>


Transparent ZnO films and coatings may be deposited onto different types of substrates by physical or chemical methods. Among the chemical approaches, dip-coating, spin-coating, flame-spray pyrolysis, and spray-pyrolysis lead to good quality dense transparent films. Spray-pyrolysis is a particularly convenient method for the deposition of ZnO films from non-expensive precursors, water or alcohol soluble, not requiring further viscosity adjustments of the solution to be sprayed. This atmospheric-pressure solution deposition route is an attractive alternative to the traditional vacuum-based physical vapor deposition techniques. Furthermore, it is easily scalable and allows controlling coating thickness avoiding several depositions followed by heat treatments, as is usual in dip- and spin-coating procedures.<sup>[11–14]</sup> This work presents a discussion on the influence of grain size on the ultraviolet light response of zinc oxide films grown by a spraying technique, towards the understanding of the electrical behavior and optimization of UV-sensor devices based on this oxide.

## 2. Experimental Section

Pure zinc oxide films were deposited on soda-lime glass substrates by spray-pyrolysis. Substrates had been previously coated with a silica (SiO<sub>2</sub>) film by dipping them in a tetraethoxysilane (TEOS) ethanolic solution. The silica film acts as a barrier against the diffusion of Na<sup>+</sup> from the substrate to the ZnO film. The influence of different precursors for ZnO on the microstructure development of thin films deposited by spray-pyrolysis has been discussed in the literature.<sup>[15]</sup> In this work, zinc acetate (4 g, Zn(OCOCH<sub>3</sub>)<sub>2</sub>·2H<sub>2</sub>O, 98%, Cicarelli) was dissolved in 40 ml of absolute ethanol (99.5%, Cicarelli), under stirring, with the aid of 2,4-pentanedione (Acac, ≥99%, Aldrich) in a 1:1 Zn:Acac molar ratio. The solution was sprayed onto 70 × 25 mm<sup>2</sup> glass substrates at 425 °C with nitrogen (1.5 bar) as carrier gas at a distance of 15 cm between nozzle and substrate.

E. A. Villegas, Prof. C. M. Aldao, Dr. L. A. Ramajo, Dr. R. Parra  
Instituto de Investigaciones en Ciencia y Tecnología de Materiales (INTEMA)  
Universidad Nacional de Mar del Plata  
Consejo Nacional de Investigaciones Científicas y Técnicas (CONICET)  
B7608FDQ Mar del Plata, Argentina  
E-mail: rparra@fi.mdp.edu.ar

Dr. R. Savu  
Centro de Componentes Semicondutores (CCS)  
Universidade Estadual de Campinas (UNICAMP)  
CP 6061 Campinas, SP, Brazil

 The ORCID identification number(s) for the author(s) of this article can be found under <https://doi.org/10.1002/pssa.201800107>.

DOI: 10.1002/pssa.201800107

The microstructure of the obtained films was characterized by means of grazing incidence-X-ray diffraction (GI-XRD) at 0.5° in a PANalytical X'Pert diffractometer running with  $K\alpha$ -Cu radiation, and scanning electron microscopy (FE-SEM) in a FEI Quanta 250 FEG microscope. Film thicknesses were determined by mechanical profilometry with a KLA Tecnor E-100 instrument. Optical transmittance was measured on the basis of UV-Visible spectra recorder with a UV-VIS-NIR Shimadzu 3600 spectrophotometer, equipped with an integrating sphere, in the 3600–200 nm range.

In order to study the electrical response of films under UV illumination, a black-chamber was equipped with two 4 W Philips 365 nm (UVA region) tube lamps, a 4-lead sample holder arranged with Ingun test probes, and a chopper between lamps and sample. It has been determined that exposing films to light of wavelength near the Urbach tail of ZnO (365 nm), ensures sufficient absorption and penetration.<sup>[16]</sup> In order to keep lamps irradiating at maximum power, they remained on during the whole measurement. The power density reaching the surface of specimen under test was measured to be 2.5 mW cm<sup>-2</sup> by means of a broad band thermopile power detector connected to a Gentec Maestro Power and Energy monitor (UP19K-15S-H5D0). Curves of photocurrent as function of time were registered by means of Rigol DM3058 and DM3062 digital multimeters. Because of the high resistivity of films, and the 5 mm distance between probes, a 20 V dc-bias was applied by means of a Siglent SPD3303D DC power supply unit. No electrodes were deposited or painted on the films surface. Measurements were carried out at room temperature not modifying the ambient atmosphere (60–70% relative humidity).

### 3. Results and Discussion

#### 3.1. Optical and Microstructural Characterization

Zinc oxide coatings of different grain size and thickness were obtained by spraying 20 (ZO20), 30 (ZO30), and 40 ml (ZO40) of precursor solution. Grain size and thickness of obtained films are shown in Table 1. The corresponding transmittance spectra in the UV-visible-NIR region in Figure 1, where the visible gap (390–750 nm) is highlighted, show that the optical transmittance in the visible region is reduced as thickness and grain size increase. It can be clearly observed that direct transmittance within the visible region is above 90% for the thinnest film, whereas it falls below 80% for the 415 nm film. A sharp absorption edge is observed, confirming the crystalline nature of films.<sup>[17]</sup> The absorption edge shifts to blue with decreasing thickness, indicating wider optical band-gaps for films with

**Table 1.** Thickness ( $t$ ), grain size ( $d$ ), sheet resistance ( $R_{sh}$ ), resistivity ( $\rho$ ), and UV-light to dark conductivity ratio ( $\sigma_{ph}/\sigma_d$ ) of ZnO films.

Sample	$t$ [nm]	$d$ [nm]	$R_{sh}$ [k $\Omega$ sq <sup>-1</sup> ]	$\rho$ [ $\Omega$ .cm]	$\sigma_{ph}/\sigma_d$
ZO20	170	120	1980	30.3	3.4
ZO30	235	230	130	3.1	1.9
ZO40	415	300	12.7	0.5	1.2

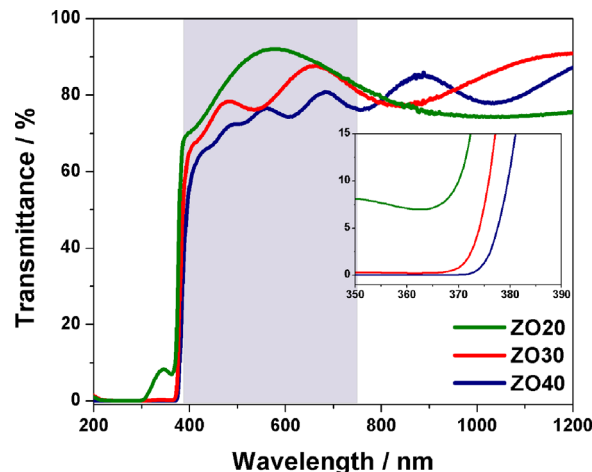


**Figure 1.** Optical transmittance curves for ZnO films. The visible region of the spectrum is highlighted. Inset shows the blueshift of the absorption edge with thickness.

smaller grains. In addition, the number of oscillations due to interference effects produced at the film/substrate interphase also increases with film thickness.

The model proposed by Swanepoel provides a method to calculate the optical constants of a film from the interference fringes.<sup>[18]</sup> The model correlates the refraction index of the film, its thickness and the fringes by means of the following equations,

$$n = \left( N + (N^2 - S^2)^{1/2} \right)^{1/2} \quad (1)$$

$$N = 2s \frac{T_M - T_m}{T_M T_m} + \frac{s^2 + 1}{2} \quad (2)$$

$$t = \frac{M\lambda_1\lambda_2}{2(\lambda_1 n_2 - \lambda_2 n_1)} \quad (3)$$

where  $n$  is the refraction index and  $t$  the thickness of the ZnO film,  $s$  is the refraction index of the substrate, and  $M$  is the number of oscillations in the curve.  $T_M$  and  $T_m$  are maximum and minimum transmittance values in the curve, respectively, which are determined by means of cubic splines fittings of each curve. The amplitude of the interference pattern ( $T_M - T_m$ ) is inversely proportional to the film thickness; then, according to Equation (2),  $n$  decreases with increasing thickness. This is in agreement with the curves in Figure 1, where the value of  $M$  is seen to increase with film thickness. For the 170 nm film,  $M = 1$  and ( $T_M - T_m$ ) takes the maximum value. On the other hand, for the 235 and 415 nm films,  $M = 2$  and 4, respectively, and ( $T_M - T_m$ ) decreases significantly.  $M$  was used in Equation (3), along with the wavelength values of two consecutive maximum and minimum peaks, and corresponding refraction indexes, in order to estimate the thickness of the film. Although thicknesses calculated from this method were 20% higher than those measured by profilometry, they were in agreement with the observed trend ZO20 < ZO30 < ZO40.

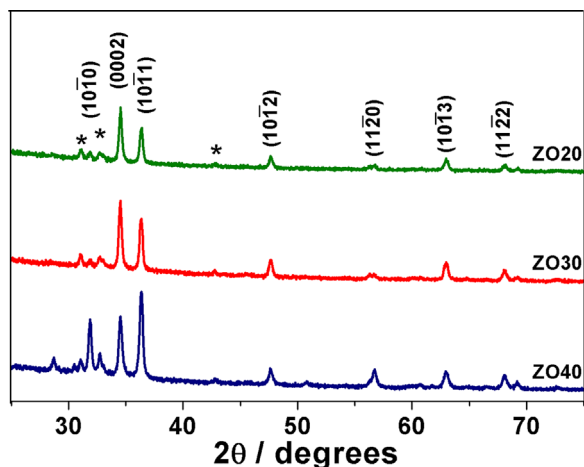


**Figure 2.** XRD patterns of ZnO films sprayed on a SiO<sub>2</sub>/glass substrate at 425 °C. Peaks with an asterisk are caused by the K<sub>β</sub> line of the Cu X-ray source.

X-ray diffraction patterns shown in **Figure 2** confirm that films are single-phase within the resolution of the technique. Diffraction peaks have been assigned to the ZnO phase according to the JCPDS file 36–1451 of the wurtzite structure. However, significant differences in relative intensities of certain peaks with respect to the mentioned file are evident. Specifically, the high intensity of the diffraction peak corresponding to the (0002) plane with respect to planes (10–10) and (10–11) in samples ZO20 and ZO30 is consistent with an enhanced anisotropic crystal growth in the *a*- and *b*-directions, perpendicular to the [0001] direction (*c* axis). Then, as far as the usual morphologies observed for ZnO nanostructures,<sup>[19,20]</sup> ZO20 and ZO30 films would be built up of hexagonal platelet-like grains, exhibiting mainly {0001} faces, rather than elongated structures or rods of hexagonal cross section. On the other hand, the changes observed in the relative intensities of planes (10–10), (10–11), and (11–20) with respect to plane (0002) in the XRD pattern of film ZO40, show a different crystal morphology revealing an inversion in the anisotropy of grains. It seems that growing in the equatorial *a* and *b* directions is overtaken by a preferential growth in the *c* direction.

Films were observed under FE-SEM magnification in order to assess the microstructure and determine grain morphology. Average grain sizes measured from images in **Figure 3**, which shows crack-free microstructures, are reported in Table 1. As shown in these images, films ZO20 and ZO30 are built of hexagonally-shaped platelets or disks, in agreement with XRD results and confirming that spraying conditions other than those reported by Htay et al. lead to this type of grains/particles.<sup>[21]</sup> Interestingly, film ZO40 is formed of larger grains which have started to grow in the *c* direction in a step-wise manner, as represented in **Scheme 1**. This is in agreement with the corresponding XRD pattern, which shows a diffraction peak corresponding to the (0002) plane of lower intensity with respect to that in samples ZO20 and ZO30, in agreement with the observations by Bo et al. for porous ZnO films.<sup>[22]</sup> Hexagonal platelets happen to grow until a limiting diameter at which they become the seed crystallites for a secondary nucleation process

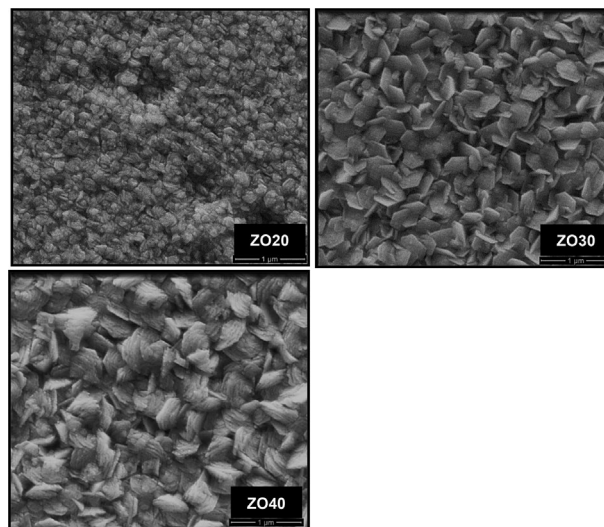
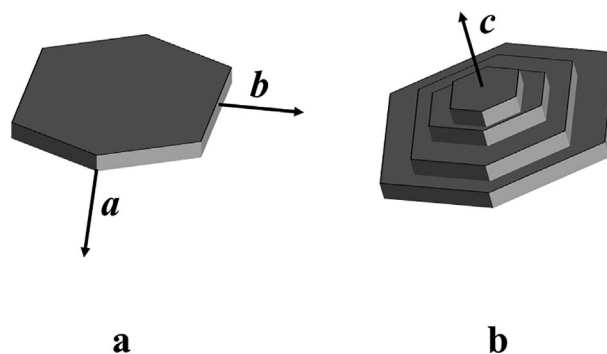


**Figure 3.** FE-SEM images of ZnO films deposited by spray-pyrolysis on glass substrates. (Bar 1 μm; Magnification 70 kX).

that takes place on {0001} faces. Then, grains in film ZO40 consist in multilayered arrangements hexagonal stacked platelets. Should more solution be sprayed on sample ZO40, further growth along the *c* axis would take place, leading to typical ZnO elongated structures of hexagonal cross section. This seems probable since the {10-10} surfaces are the most stable ones and the {0001} exhibit the highest surface energy of the low-index planes. Then, crystal growth is favored in the [0001] direction, ending in rods with minimized and maximized areas for {0001} and {10-10} faces, respectively.<sup>[20,23]</sup>

### 3.2. Electrical Properties and Photoconductivity

Zinc oxide films presented high sheet resistance (*R*<sub>sh</sub>) and resistivity (*ρ*) values as shown in Table 1, where the dependence on grain size is clearly observed. As grain size increases, lower resistance for conductivity is measured. Larger grains build films with lower density of potential barriers against carrier conduction. Furthermore, these measured values should be analyzed



**Scheme 1.** Schematic diagram of grain morphologies observed in samples ZO20 and ZO30 (a), and ZO40 (b), indicating preferential growing directions in each case.

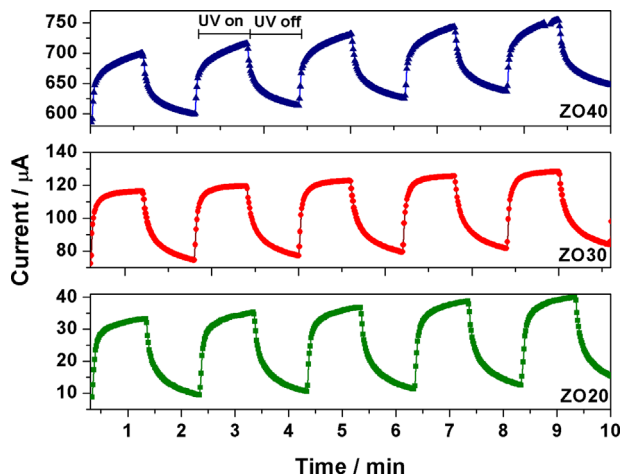


**Figure 4.** Time dependence of current under dark and UV illumination conditions for ZnO films.

under consideration of the observed hexagonal platelet grain morphology, which may not be optimal for electrical contact between grains, and is another contribution to the naturally high  $R_{sh}$  that characterizes undoped ZnO films.

As to the response of the films to UV light, curves of photocurrent registered in time under dark and illumination (365 nm light) conditions are shown in **Figure 4**. The photoresponse of ZnO films is attributed to the electronic process that involves the reduction in the barrier height due to electron-hole pairs photogenerated in a process related to oxygen exchange (photodesorption-quimisorption) at the grain boundaries (bulk process) or grain surface (surface process). Under normal ambient atmosphere, oxygen quimisorbs at the surface of grains and captures electrons from the conduction band, thus creating a depletion region and a potential barrier which causes an increase in the resistivity of the film. Upon illumination with light of wavelength comparable to the band-gap, holes migrate to the surface where they neutralize negatively charged oxygen species ( $O_2^-$ ) promoting the photodesorption of  $O_2(g)$ , finally decreasing the barrier height. Electrons are released to the conduction band, resulting in a significant reduction of film resistivity.<sup>[24–26]</sup>

**Figure 4** shows that the conductivity of all samples was enhanced when illuminated with 365 nm wavelength light, followed by a decay after closing the shutter in a reproducible process. The most intense response, in terms of the ratio of conductivity under dark and UV-light conditions ( $\sigma_{ph}/\sigma_d$ ) corresponds to sample ZO20, the most resistive film with the smallest average grain size (120 nm), which showed a  $\sigma_{ph}/\sigma_d$  ratio of 3.4. A fast decay to the initial dark current value is also observed, suggesting a quick readsorption of oxygen to the surface of grains. The least intense response ( $\sigma_{ph}/\sigma_d = 1.2$ ) was registered for film ZO40 with the largest average grain size (300 nm), which also showed the highest dark-current and a slow increase in current when illuminated, with respect to samples ZO20 and ZO30. Longer times are needed for this film in order to completely recover the initial dark current value by means of the adsorbance and diffusion of molecular

oxygen. **Figure 5** shows a simplistic model that aids explaining the UV light-sensitivity trend ( $ZO20 > ZO30 > ZO40$ ) observed as grain size increases and sheet resistance decreases. Small grains are characterized by relatively wider depletion regions with respect to large grains. In fact, small grains may be fully depleted presenting overlapped potential barriers.<sup>[22,27]</sup> On the other hand, large grains are only surface-depleted. Then, considering potential barriers with equal profiles, there is a larger electron depleted volume fraction in smaller grains, which determines lower dark currents. Changes in the concentration of surface states induced by UV light and excess oxygen desorption, provoke a more intense response in films with small grains. This surface effect does not affect significantly the overall resistance of films composed of large grains.

The above findings deserve a deeper discussion. For the sake of simplicity, we will assume uniform photogeneration  $G_{ph}$  and cubic grains of side  $d$ . We also assume that all recombination occurs at the grain boundaries, that is, at the faces of the cube. This implies that the total photogeneration inside a grain reflects as a current density  $J_{ph}$  given by

$$6d^2 J_{ph} = eG_{ph}d^3 \quad (4)$$

The surface of a grain constitutes a semiconductor junction that behaves like a diode with a rectifying current-voltage characteristic. When the junction is illuminated, its current-voltage characteristic can be approximated as the sum of the dark current and the short circuit photocurrent. This is known as the superposition approximation, which is reasonable in our case.<sup>[28]</sup> Thus, the net current density at the junction is

$$J(V) = J_0 \left( e^{\frac{eV}{kT}} - 1 \right) - J_{ph} \quad (5)$$

where  $V$  is the applied voltage,  $J_0$  is the reverse bias saturation current, and  $J_{ph}$  is the current density due to illumination, the photocurrent density.

The conductivity of a single junction can be derived using Equation (5). In the dark,  $J_{ph} = 0$ ,

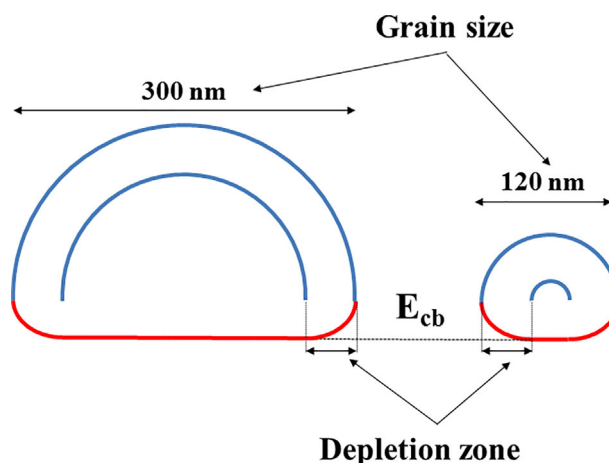


**Figure 5.** Schematic diagram of the depletion zone and voltage barrier in grains of different size.

$$\sigma_d = \frac{dJ}{dV} \Big|_{V=0} = J_0 \frac{e}{kT} \quad (6)$$

and, under illumination, the conductivity is

$$\sigma_{ph} = \frac{dJ}{dV} \Big|_{V=V_{OC}} = J_0 e^{\frac{eV_{OC}}{kT}} \frac{e}{kT} \quad (7)$$

where  $V_{OC}$  is the open circuit voltage.

Therefore, with Equations (6) and (7), we can determine the ratio between conductivities under illumination and in the dark as a function of  $J_{ph}$  and  $J_0$

$$\frac{\sigma_{ph}}{\sigma_d} = e^{\frac{eV_{OC}}{kT}} = 1 + \frac{J_{ph}}{J_0} \quad (8)$$

Assuming that electrical conduction is mostly controlled by intergrains, the resistivity of a polycrystal must be proportional to the density of intergrains. Then, considering Equation (6), the resistivity must be inversely proportional to the grain size and  $J_0$ . Thus, we can write

$$J_0 = \frac{C}{\rho d} \quad (9)$$

where  $C$  is a constant.

Finally, with Equation (8) and using the results of Equations (4) and (9)

$$\frac{\sigma_{ph}}{\sigma_d} = 1 + \frac{J_{ph}}{J_0} = 1 + K\rho d^2 \quad (10)$$

where  $K$  is a constant that includes the photogeneration and constant  $C$ . Equation (10) reveals the dependence of the relative conductivity, under illumination and in the dark, on the film resistivity and grain size. Even though we do not have the value of  $K$ , we can check the consistency of the found values of  $\sigma_{ph}/\sigma_d$  for different samples. Indeed, by applying Equation (10) to ZO20 sample we can determine  $K$ .

$$K = \left( \frac{\left( \frac{\sigma_{ph}}{\sigma_d} - 1 \right)}{\rho d^2} \right)_{ZO20} \quad (11)$$

With this value of  $K$ ,  $\sigma_{ph}/\sigma_d$  for samples ZO30 and ZO40 are 1.9 and 1.25, respectively. Thus, the model predicts very well the conductivity dependence on grain size observed experimentally.

After the previous analysis, an increase in the UV photoresponse of film ZO20 may be expected by optimization of grain size. For instance, a further decrease in grain size might be followed by an increase of the  $\sigma_{ph}/\sigma_d$  ratio. However, this will be so as far as the assumptions of the model are met and the film resistivity keeps increasing.

## 4. Conclusions

The microstructure and electrical properties of non-doped zinc oxide thin films deposited by spray-pyrolysis have been studied. The

grain size was modified (from 120 to 300 nm) by variations in the volume of precursor solution sprayed onto the substrate. Moreover, the grain morphology changed significantly after spraying growing volumes of the precursor, changing from platelets towards elongated 3D grains. Under UV-light illumination, the UV-light to dark conductivity ratio was seen to decrease with grain size. Small grains lead to the low dark-currents needed for high photoresponse. A model that accurately predicts the relative conductivity of ZnO films in the dark and under illumination, as a function of grain size and resistivity, was proposed. It is expected that these results may be useful for the development and microstructure engineering of ZnO-based UV-light sensors.

## Acknowledgements

Thanks are due to V. Fuchs for XRD measurements and to M. Lere for equipment upgrade and design. This work was carried out with the financial support of ANPCyT (PICT'15 2305), CONICET, and University of Mar del Plata (Argentina).

## Conflict of Interest

The authors declare no conflict of interest.

## Keywords

spray-pyrolysis, thin films, ultraviolet photodetectors, zinc oxide

Received: February 9, 2018

Revised: March 21, 2018

Published online:

- [1] C. Klingshirn, *ChemPhysChem* **2007**, *8*, 782.
- [2] E. Mammadov, N. Naghavi, Z. Jehl, G. Renou, T. Tiwald, N. Mamedov, D. Lincot, J.-F. Guillemoles, *Thin Solid Films* **2014**, *571*, 593.
- [3] E. Ochoa-Martínez, E. Navarrete-Astorga, J. Ramos-Barrado, M. Gabás, *Appl. Surf. Sci.* **2017**, *421*, 680.
- [4] A. B. Djurišić, Y. H. Leung, *Small* **2006**, *2*, 944.
- [5] Ü. Özgür, Y. I. Alivov, C. Liu, A. Teke, M. A. Reshchikov, S. Doğan, V. Avrutin, S.-J. Cho, H. Morkoç, *J. Appl. Phys.* **2005**, *98*, 041301.
- [6] R. Savu, R. Parra, E. Joanni, B. Jančar, S. A. Eliziário, R. de Camargo, P. R. Bueno, J. A. Varela, E. Longo, M. A. Zaghete, *J. Cryst. Growth* **2009**, *311*, 4102.
- [7] C. Soci, A. Zhang, B. Xiang, S. A. Dayeh, D. P. R. Aplin, J. Park, X. Y. Bao, Y. H. Lo, D. Wang, *Nano Lett.* **2007**, *7*, 1003.
- [8] J. Dai, C. Xu, J. Guo, X. Xu, G. Zhu, Y. Lin, *AIP Adv.* **2013**, *3*, 062108.
- [9] S. Li, W. Tang, X. Xu, M. Cao, Y. Jin, X. Guo, *Phys. Status Solidi A* **2014**, *211*, 2184.
- [10] Q. Liu, M. Gong, B. Cook, P. Thapa, D. Ewing, M. Casper, A. Stramel, J. Wu, *Phys. Status Solidi A* **2017**, *214*, 1700176.
- [11] P. S. Patil, *Mater. Chem. Phys.* **1999**, *59*, 185.
- [12] R. M. Pasquarelli, D. S. Ginley, R. O'Hayre, *Chem. Soc. Rev.* **2011**, *40*, 5406.
- [13] A. Nakaruk, C. C. Sorrell, *J. Coat. Technol. Res.* **2010**, *7*, 665.
- [14] F. A. Garcés, N. Budini, R. D. Arce, J. A. Schmidt, *Thin Solid Films* **2015**, *574*, 162.
- [15] R. Romero, D. Leinen, E. A. Dalchiale, J. R. Ramos-Barrado, F. Martín, *Thin Solid Films* **2006**, *515*.

- [16] P. Fuchs, J. Steinhäuser, Y. E. Romanyuk, A. N. Tiwari, *Phys. Status Solidi A* **2017**, 214, 1600853.
- [17] A. Nebatti, C. Pflicht, B. Curdts, B. Atakan, *Mater. Sci. Semiconductor Processing* **2015**, 39, 467.
- [18] R. Swanepoel, *J. Phys. E: Sci. Instrum.* **1983**, 16, 1214.
- [19] S. Cho, S.-H. Jung, K.-H. Lee, *J. Phys. Chem. C* **2008**, 112, 12769.
- [20] B. Ludi, M. Niederberger, *Dalton Trans.* **2013**, 42, 12554.
- [21] M. T. Htay, Y. Hashimoto, K. Ito, *Jpn. J. Appl. Phys.* **2007**, 46, 440.
- [22] R. Bo, N. Nasiri, H. Chen, D. Caputo, L. Fu, A. Tricoli, *ACS Appl. Mater. Interfaces* **2017**, 9, 2606.
- [23] M. Wang, S. H. Hahn, J. S. Kim, J. S. Chung, E. J. Kim, K.-K. Koo, *J. Cryst. Growth* **2008**, 310, 1213.
- [24] D. H. Zhang, *J. Phys. D Appl. Phys.* **1995**, 28, 1273.
- [25] S. Kumar, G.-H. Kim, K. Sreenivas, R. P. Tandon, *J. Phys.: Condens. Matter* **2007**, 19, 472202.
- [26] Y. He, W. Zhang, S. Zhang, X. Kang, W. Peng, Y. Xu, *Sens. Actuators A* **2012**, 181, 6.
- [27] F. Schipani, M. A. Ponce, E. Joanni, F. J. Williams, C. M. Aldao, *J. Appl. Phys.* **2014**, 116, 194502.
- [28] J. Nelson, *The Physics of Solar Cells*. Imperial College Press, UK, London **2005**, Chapter 1.